Pulsed-laser induced transient phase transformations at the Si–H_2O interface

A. Polman and W. C. Sinke
FOM-Institute for Atomic and Molecular Physics, Kruislaan 407, 1098 SJ Amsterdam, The Netherlands

M. J. Uttormark and Michael O. Thompson
Department of Materials Science, Cornell University, Ithaca, New York 14853

(Received 14 November 1988; accepted 22 March 1989)

Phase transformations at the Si–H_2O interface, induced by nanosecond pulsed laser irradiation, were studied in real time. Si samples were irradiated using a 4 ns pulse from a *Q*-switched frequency-doubled Nd:YAG laser while immersed in the transparent liquid. Using time-resolved conductivity and reflectivity techniques, in combination with modeling of optical parameters and heat flow, transient processes in the Si, the H_2O, and at the interface have been unraveled. In the liquid, local rapid heating occurs as a result of heat flow across the interface, and formation of a low-density steam phase occurs on a nanosecond timescale. Expansion of this phase is followed by a collapse after 200 ns. These rapid phase transformations in the water initiate a shock wave with a pressure of 0.4 ± 0.3 kbar. Transient phase transformations and the heat flow into the water during the laser pulse influence the energy coupling into the sample, resulting in an effective laser pulse shortening. The pulse shortening and the additional heat flow into the water during solidification result in a 30% enhancement of the solidification velocity for 270 nm deep melts. Cross-section transmission electron microscopy data reveal that the Si surface is planar after irradiation and is inert to chemical reactions during irradiation. Recent experiments described in the literature concerning pulsed-laser induced synthesis at the solid-liquid interface are reviewed and discussed in the context of the fundamental phenomena presently observed.

I. INTRODUCTION

Pulsed-laser irradiation provides a convenient means to induce rapid and often nonequilibrium phase transformations in solids. During the last ten years especially pulsed-laser irradiation of semiconductors has been extensively investigated and the nature of the various processes occurring is now well established[1–5]: during irradiation with a nanosecond laser pulse, energy is absorbed in a shallow surface layer with subsequent melting of the surface and penetration into the solid. Following the laser pulse, the molten layer solidifies as heat is conducted into the substrate. Depending on the experimental conditions the surface layer solidifies to an amorphous, polycrystalline, or epitaxial monocrystalline phase. Various melting and solidification scenarios including segregation and trapping of impurities,[6–9] 'internal' melt nucleation,[10] surface solidification,[11] and 'explosive' crystallization[12–15] have been developed. These experiments have given insight into several fundamental materials properties and nonequilibrium process parameters.[16–20]

Most investigations have been devoted to laser irradiation at the solid-vacuum or solid-air interface. In those cases, the heat-flow processes can be modeled with a one-dimensional calculation[21,22] under the constraint of no thermal or chemical interaction between the sample and the ambient medium. The main focus of these experiments was on the phase transformations of the solid.

For the past five years, the solid-gas and solid-vapor reactive systems have become a topic of research for pulsed-laser processing, mainly for technological reasons. Using pulsed-laser irradiation it is possible to induce chemical reactions at these interfaces. Under these conditions the gas or vapor itself does not usually influence the thermal transport phenomena in the solid. A variety of experiments have been performed, concerning melting of a surface layer of the substrate followed by incorporation of species from the gas. Stable and metastable compound films with submicron thickness,[23–26] as well as shallow doped surface layers,[27–29] can be synthesized using these techniques.

Recently, laser irradiation at the solid-liquid interface has become an important new alternative also. In this case, a shallow surface layer of the solid is melted using a pulsed-laser incident through a surrounding liquid ambient. From an applied point of view, this technique offers interesting possibilities similar to those of the solid-gas or solid-vapor reactions: reactive species from the liquid can be incorporated in the locally molten solid.[30–40] However, because of the high density in the liquid the reaction efficiency is much higher. In addition, the close thermal coupling between the two media causes the heat flow characteristics in the solid material to be modified by the presence of the liquid medium. Hence, the quench rate to the solid phase can be enhanced by this technique.[41] This is

important since the quench rate is the primary parameter controlling the segregation and trapping of impurities[1,6,8] and the structural phases of the material following solidification.[5,42,43] Until today, results concerning laser irradiation at the liquid-solid interface have been reported for the Si–, Fe–, Ti–, Ta–, and Be–H_2O systems, the Ti–, Zr–, Hf–, V–, Nb–, Be–, and Ta–liquid N_2 systems, and the Ti–NH_3, Si–$SbCl_3$, Si–$C_{12}H_{27}O_4P$, and W–C_6H_6 systems.[30–41] However, many questions concerning the fundamental transient processes at the solid-liquid interface remain unanswered.

Apart from the technological need to elucidate the interface reactions, there is a fundamental interest in laser irradiation at the liquid-solid interface. Using nanosecond pulses the liquid near the liquid-solid interface will be heated far from equilibrium and it is interesting to follow the processes in the liquid in real time. Additionally, the quench rate enhancement in the solid is interesting from a theoretical viewpoint as this rate is central to the study of nonequilibrium liquid-solid interface dynamics.

In the present experiments, phase transformations were studied during pulsed-laser irradiation at the Si–H_2O interface. This system is chosen as a model system because the optical and thermal properties of the two media are well known. Furthermore, in this system the Si does not react with the H_2O. These properties enabled us to unravel the distinct transformations in the liquid from those in the solid. Using transient reflectance techniques and modeling of heat flow and optical parameters, we studied local ultra-rapid heating effects in the water. Transient vapor formation, -expansion, -collapse, and subsequent shock wave formation effects have been investigated. In addition, the influence of phase transformations in the water on the laser energy coupling into the sample was studied. Time-resolved conductivity measurements were used to study the influence of the presence of the water layer on the quench rate in the molten solid. The observed phenomena are analyzed in terms of standard heat flow. The results are applied to other experiments described in the literature concerning laser-induced synthesis at the liquid-solid interface.

II. EXPERIMENTAL

Both bulk Si (100) and 500 nm Silicon On Sapphire (SOS) samples were used in these experiments. The SOS samples were patterned photolithographically to yield samples for transient conductance measurements. The transient conductance technique,[44] utilizing the 30-fold increase in conductivity of Si upon transformation to the liquid phase,[45] monitors the molten Si thickness in real time. Samples were positioned in a transparent reservoir which was filled with de-ionized water at room temperature. A schematic diagram of the setup is shown in Fig. 1.

Samples were irradiated with a single pulse from a *Q*-switched frequency-doubled Nd:YAG laser operating at

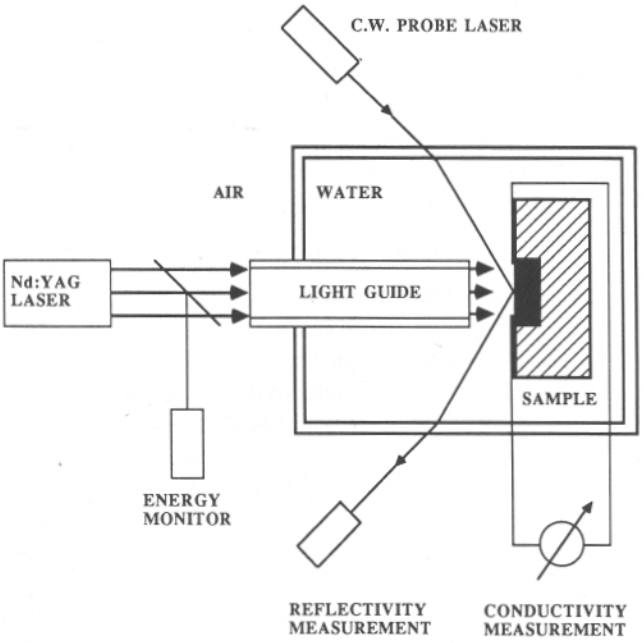

FIG. 1. Schematic drawing of the experimental setup.

$\lambda = 532$ nm and a pulse width of 4 ns Full Width at Half-Maximum (FWHM). Laser energy was coupled into the sample through a quartz guide diffusor.[46] All conductance measurements were performed at a sample-to-lightguide distance of 0.6 mm with an estimated nonuniformity of ±5% over the 6 mm diameter of the spot. No chemical etch treatment was applied to the samples before irradiation.

During irradiation, the optical properties of the Si-water interface were probed at a glancing angle of 79° relative to the surface normal by transient optical reflectance[47] using a continuous wave semiconductor laser operating at $\lambda = 780$ nm. Both the *s* (perpendicular) and *p* (parallel) polarizations were monitored. The reflected intensities were monitored through narrow-band transmission filters using a fast photo-diode. Although the conductance measurements were performed on SOS samples, reflectivity measurements had to be performed on bulk single crystal samples to avoid unwanted interference effects of reflections from the three interfaces of SOS samples. To study acoustical effects in the water, the sample-to-lightguide distance was varied in the range 0.6–5.0 mm. For these distances a nonuniformity of ±5% was estimated for the center 1 mm diameter area in the spot on which reflectance measurements were actually employed. Both conductance and reflectance data were acquired with >500 MHz bandwidth. Reference samples were irradiated in air in the same configuration prior to the introduction of water.

The relative laser energy incident on the lightguide was measured within 5% using calorimetry. It should be noted that the energy at the output end of the lightguide in air is different from that in water, as different conditions for internal reflection in the lightguide hold for the two

situations. Determination of the absolute value of incident energy under water was not possible, and hence a direct comparison of the energy densities incident in water and air could not be made.

Cross-sectional Transmission Electron Microscopy (TEM) was employed to study microstructural changes in the samples following irradiation.

III. RESULTS

A. Phase transformations in the Si

1. Transient conductivity

Comparisons of the melt and solidification dynamics for SOS samples irradiated in air and in water are shown in Fig. 2. The two transients shown in Fig. 2(a) were selected to show comparable maximum melt depth. The inset in the figure shows an enlarged view of the melt turn-around points. Figure 2(b) shows the corresponding liquid-solid interface velocities during solidification obtained by numerical differentiation of the curves in Fig. 2(a). The figure shows that the melting and resolidification behavior for irradiation under water is qualitatively similar to that in air: rapid melt-in followed by a slower solidification transient. However, for this peak melt depth of 270 nm the regrowth behavior differs in the two experimental situations. Firstly, the maximum quench velocity is enhanced from 5.2 m/s to 6.8 m/s. As a consequence, the total duration of the melt, obtained by extrapolating the slope in the straight part of the transients in Fig. 2(a) to zero thickness, is reduced by 25%. Tails observed in Fig. 2(a) for $t > 60$ ns are attributed to slight inhomogeneities in the irradiation energy density and finite conduction in the underlying hot solid Si. Secondly, a small but significant difference in melt-in behavior is observed: the peak melt depth occurs earlier in time for irradiation under water. This can be seen in both the inset in Fig. 2(a) and the intercept with the abscissa of the transients in Fig. 2(b). This phenomenon was found to occur reproducibly over a large energy range.

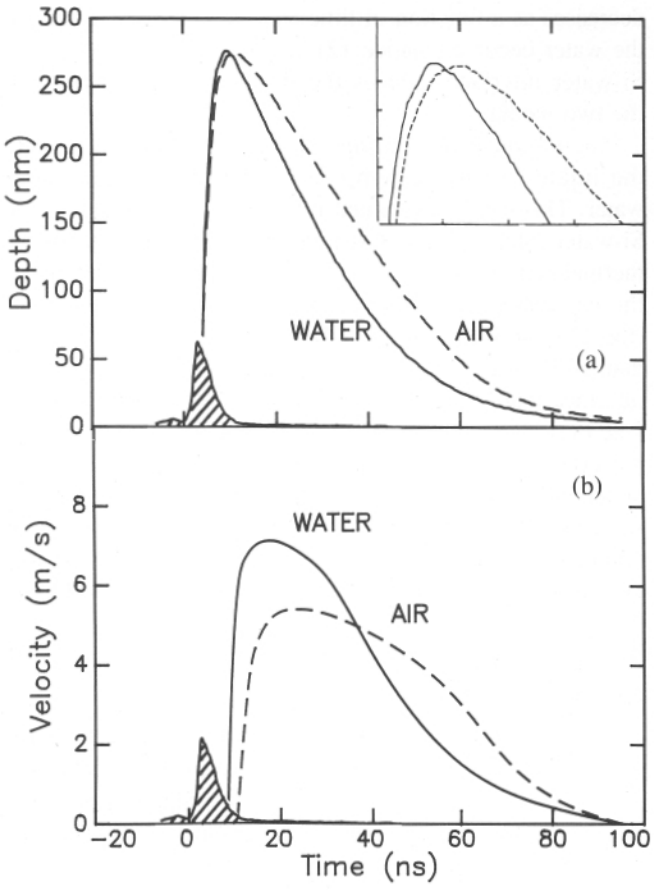

FIG. 2. (a) Melt depth transients for samples irradiated in air (dashed) and under water (solid). The hatched region indicates the relative timing of the laser pulse. (b) Liquid-solid interface velocities calculated from the curves in (a).

The melting and solidification behavior was studied for an extended range of energy densities. Figure 3 shows the peak melt depth, determined from conductance measurements, for samples irradiated under water and in air as a function of the energy incident on the lightguide. The behavior of melt depth versus energy for samples irradiated in air is similar to that in earlier work: above a threshold energy necessary to induce surface melting, the melt depth increases linearly with laser energy.[48] For samples irradiated under water the behavior is qualitatively the same. As previously noted, absolute values in laser energy cannot be compared because of differences in energy coupling in the two configurations.

Figure 4 shows the maximum regrowth velocity as a function of peak melt depth for a series of samples irradiated in air and water. The use of peak melt depth as the abscissa minimizes the effect of differences in the energy coupling in the two configurations. The behavior of samples irradiated in air is again similar to earlier work.[48] For shallow (<150 nm) melts, the effect of the water is insignificant compared to the scatter of the data. For deep melts, however, the regrowth velocities under water are

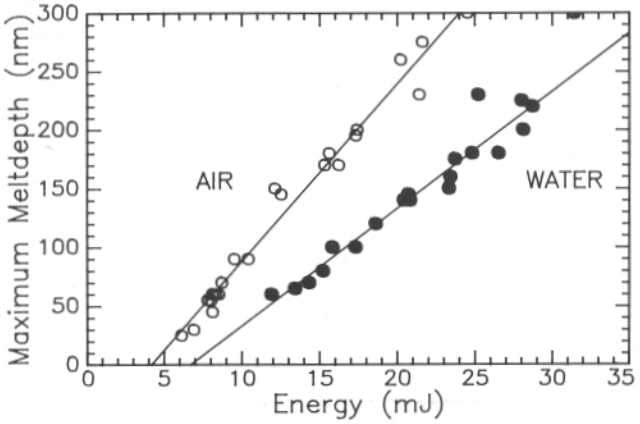

FIG. 3. Maximum melt depth as a function of laser energy incident at the lightguide entrance (see text). Results for irradiation in air (open circles) and water (closed circles) are compared.

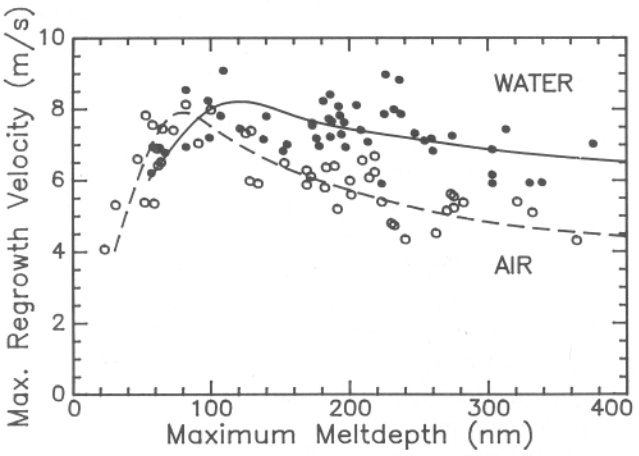

FIG. 4. Maximum regrowth velocities as a function of maximum corresponding melt depth for a series of samples processed at various energy densities either in air (open circles, dashed line) or in water (closed circles, solid line).

substantially enhanced above those for the same melt depth in air, increasing to approximately 30% for 300 nm melts.

2. Heat flow calculations

First order one-dimensional heat flow estimates were made to model the heat transport at the Si–H_2O interface and the influence on the melting and solidification processes in the Si.

a. Heat flow during the laser pulse: melt-in. A characteristic limit of the heat flow from Si to water during the laser pulse can be estimated from the thermal conductivity in water and the heat diffusion length on the laser pulse timescale. When we assume a temperature gradient of 2000 K (a characteristic temperature rise for the Si surface for irradiation in air[1]) over the thermal diffusion length after 10 ns we find, using thermal data for water at the boiling temperature, a heat flow of 3×10^6 W/cm^2 into the water. At an energy density of 1 J/cm^2 the peak laser intensity is $I = 9 \times 10^7$ W/cm^2. Hence heat flow into the water can have an influence on the energy coupling into the sample near the tail of the laser pulse.

b. Heat flow after the laser pulse: solidification. For laser irradiation of Si immersed in water the solidification velocity v is given to first approximation by

$$v \cdot \Delta H = \kappa \cdot (\partial T/\partial z) + Q\,, \qquad (1)$$

where $(\partial T/\partial z)$ is the temperature gradient in the solid just behind the moving Si liquid-solid interface, ΔH is the enthalpy of melting, and κ is the thermal conductivity of the solid. Q represents the heat flow to the water. For a given experimental configuration, the thermal gradient is determined by 'intrinsic' parameters such as the laser absorption depth, pulse length, and thermal properties of the substrate as well as by the thermal history of the material during the experiment. For a shorter laser pulse, which results in a larger thermal gradient after melt-in, the solidification velocity is larger.

An upper estimate of the heat flow into the water through the liquid Si top layer can be evaluated from the observed enhancement in solidification velocity if it is assumed that this enhancement is completely due to the Q term in Eq. (1). For the peak melt depth of 270 nm (Fig. 2) the difference in quench rate Δv between the two cases studied is 1.6 m/s. According to Eq. (1) this corresponds to an energy release from the Si into the water during solidification of $\Delta v \cdot \Delta H = 6 \times 10^5$ W/cm^2. Thus for the integral solidification duration of 40 ns (see Fig. 2) 0.02 J/cm^2 (approximately 10% of the coupled laser power) is transported to the water. This value is equal to the amount of energy necessary to heat a water layer with a thickness of 80 nm to 100 °C and vaporize it.[49] The thermal diffusion length in water below the boiling point after 40 ns is 100 nm. Therefore indeed it seems reasonable to assume that a water layer with this thickness can be heated and vaporized. This will be discussed later.

The heat flow from the Si into the water *after the laser pulse* calculated in this section is lower than the estimated initial heat flow *during the pulse* (previous section). This can be understood from the fact that (1) heat diffusion decreases as a function of time as temperature gradients in the water become smaller, (2) a formed steam layer at the Si-water interface reduces the thermal coupling between the two media.

c. Liquid undercooling. It is interesting to estimate the liquid Si surface temperature during melting under water. This can be evaluated from the heat flow across the Si-water interface calculated above. Assuming a Si liquid thermal conductivity of 1.4 W/cm · K,[48] it follows that for the calculated heat flow of $\Delta v \cdot \Delta H = 6 \times 10^5$ W/cm^2 (for 270 nm deep melts) the Si surface is undercooled less than 10 K with respect to the Si liquid-solid interface. This interface itself is undercooled since the liquid-solid interface moves in response to this undercooling with respect to the crystalline Si melting temperature. Using the known undercooling-velocity relation of 17 K/(m/s),[50–52] the observed solidification velocity under water of 6.8 m/s can be related to an interface undercooling of 115 K. The total surface undercooling is then 125 K. This will be discussed later.

B. Phase transformations in the water

1. Transient reflectivity

To study the phase transformations in the water near the Si-water interface in real time, transient reflectance measurements were employed. Optical properties near the interface depend on pressure, temperature, and phases of these media and thus measurement of the reflectance, in combination with proper modeling, enables one to monitor these quantities in real time. Figure 5 shows typical reflectivity transients of the Si-water interface at an energy density above the melt threshold. Figure 6 shows the transient

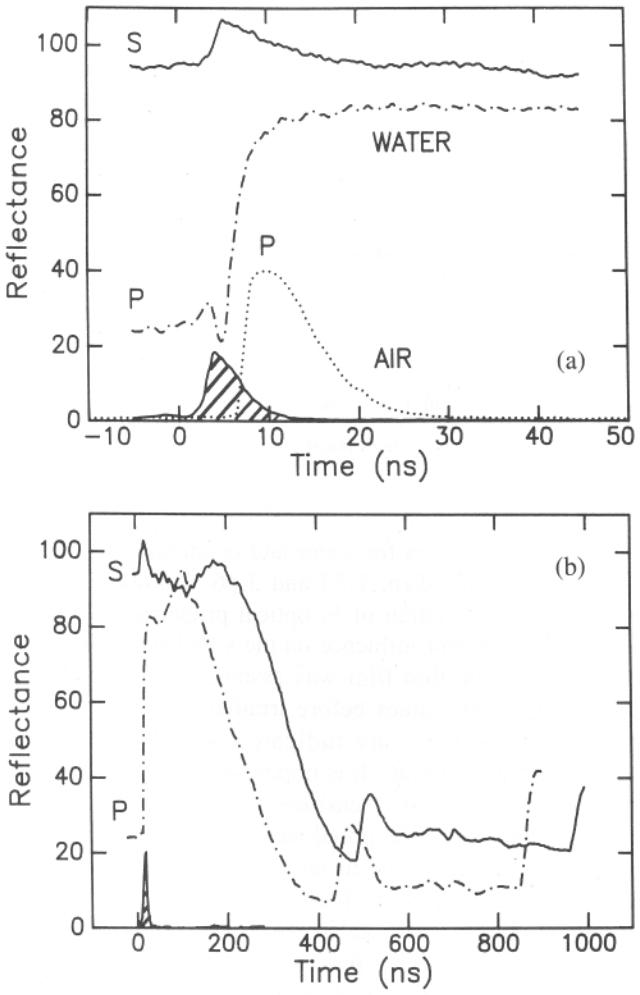

FIG. 5. Transient reflectivity traces for s and p polarizations of the cw laser measured on crystalline Si (100) upon irradiation under water (solid and dashed) and in air (dotted) are shown for short (a) and for long (b) times. Uncertainty in absolute reflectivity levels is ±4% and −4/+17% for s and p, respectively. The hatched regions indicate the relative timing of the laser pulse.

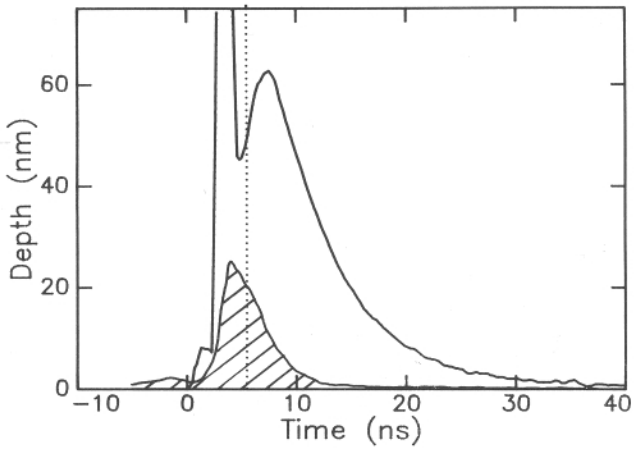

FIG. 6. Transient conductance measurement recorded at the same energy density as used in the reflectance measurements of Fig. 5. The hatched region indicates the relative timing of the laser pulse. The off-scale signal left of the vertical dotted line mainly represents the photocarrier contribution to the conductivity and does not signify real melting.

conductance trace measured on an SOS sample irradiated at a corresponding energy density. Comparable energy densities between SOS and bulk samples were obtained by comparison of melt and reflectivity behavior in air and under water of SOS and bulk samples. The peak melt depth is ≈65 nm and the total melt duration ≈15 ns.

Figure 5(a) shows the short-time (0–50 ns) reflectivity behavior. The reflectance of p polarized light on a sample irradiated in air under comparable conditions is also shown for comparison. The well-known high reflectivity plateau, corresponding to the duration of the Si surface melt, is observed in air. Under water, however, the reflectance shows considerably different structure. For p polarized light, the reflectance increases near the end of the laser pulse and remains near 100% for a time much longer than the surface melt duration. The s polarized reflectance changes only slightly during the laser pulse and also remains near 100%.

The long-term (0–1000 ns) reflectivity behavior under water is shown in Fig. 5(b). After 200 ns, both s and p reflectances decrease; however, a variety of small changes in the reflectance are observed later in time. The precise structure of these oscillations was found to change with the distance between light diffusor and sample, which will be discussed further later. The reflectivity returns to its initial value after several microseconds.

Additional optical measurements were performed on a microsecond timescale (Fig. 7). The figure shows an initial decrease in s reflectivity as was observed in Fig. 5(b) at t = 200 ns. The energy density for this figure was slightly below the surface melt threshold. At this energy density, 800 ns is required for the reflectivity level to return to the initial level. After a delay time of 2.1 μs, however, the dip in s reflectivity "echos" back and after another 2.1 μs a second "echo" is observed. This delay time was found to be dependent on the sample-diffusor distance. Delay times were determined for a number of measurements performed at several sample-diffusor distances and are presented in Fig. 8. The round trip distances from sample to diffusor were divided by the corresponding delay times, resulting in an average apparent propagation velocity of 1540 ± 40 m/s. This value is close to the velocity of sound in water[49] and will be discussed later on.

2. Optical modeling

Analysis of the reflectivity measurements was done using optical modeling techniques. It was assumed that transient transformations such as changes in pressure, temperature, and phase occur in the water at or near the Si-water interface. These transformations correspond to changes in optical parameters (i.e., refractive index). For analysis such variations are assumed to occur in a thin layer at the interface with a uniform composition. In reality the physi-

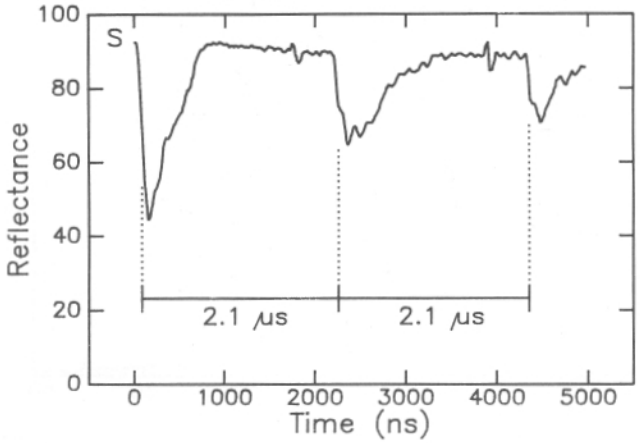

FIG. 7. Transient reflectivity traces for the *s* polarization of the probe laser. Distance sample-diffusor was 1.6 mm. The peak of the laser pulse occurs at $t = 0$ ns.

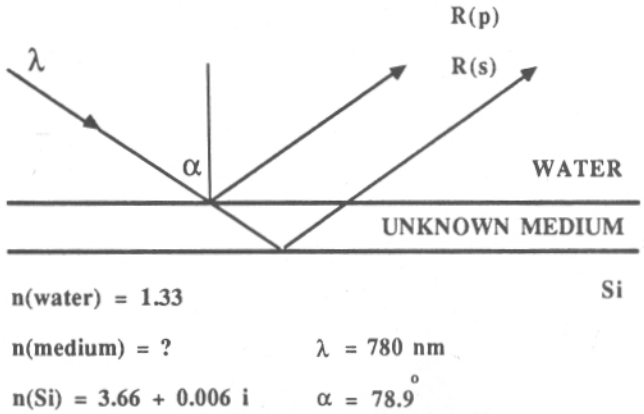

FIG. 9. Geometry used for the optical model calculations.

cal system might be more complicated, but these calculations allow the trends in the reflectivity behavior to be understood. The geometry used is given schematically in Fig. 9. Standard calculations for optical reflectivity of an ambient/thin film/substrate system[53] were used to calculate the reflectivity for a probe laser beam, reflected at this interface structure. Here the thin film represents the region in the water where the transient transformations are expected. In the simulations the *s* and *p* reflectivity are calculated as a function of refractive index and thickness of the thin film.

a. Reflectivity simulations. Figure 10 shows simulations of reflectivity as a function of refractive index in the thin film for a film thickness much thicker than the probe laser wavelength in the film. The reflectivity is very sensitive to small changes in film thickness due to interference effects in the film. In reality the interfaces will not be perfectly planar and coherence will be lost. Hence an average behavior is expected which is obtained in the simulation by averaging over a properly chosen thickness range. Complex refractive indices for water and crystalline Si at room temperature were taken: 1.33 and 3.66 + 0.006i, respectively.[49,54] The variation of Si optical properties with temperature has a minor influence on the simulated curves. No absorption in the thin film was assumed. The calculated initial reflectivity values before irradiation (index film = index water = 1.33) are indicated by arrows and the dashed line in the figure. It is important to notice that the *p* reflectance is especially sensitive to a *decrease* in refractive index relative to the initial value, whereas the *s* reflectance is also sensitive to an *increase* in index. As can be seen from the simulations, for a refractive index of the thin film well below 1.30 total reflection of the probe laser beams is expected. Under these conditions the probe laser is fully reflected at the water/thin film interface and does not monitor the Si surface. This is true only for film thicknesses larger than several probe laser wavelengths in the film.

An additional simulation was performed to calculate the influence of film thickness on the reflectivity. Figure 11 shows the calculated *p* reflectivity as a function of layer thickness for film indices in the range 1.1 to 1.33. As

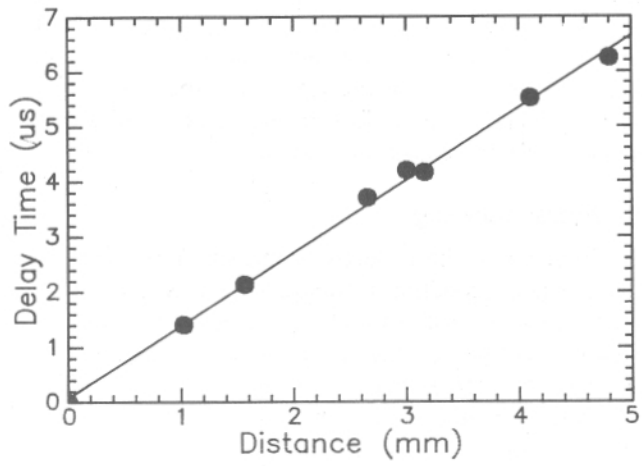

FIG. 8. Delay times for several diffusor-sample distances (see Fig. 7).

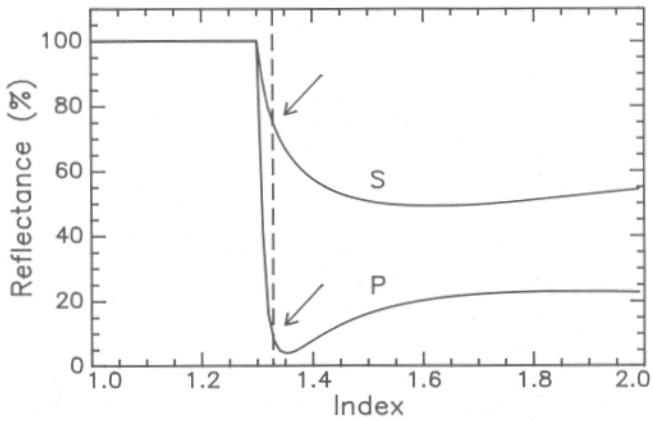

FIG. 10. Calculated reflectivity for an ambient/thin film/Si system as a function of the refractive index of the thin film (see text) for *s* and *p* polarized light.

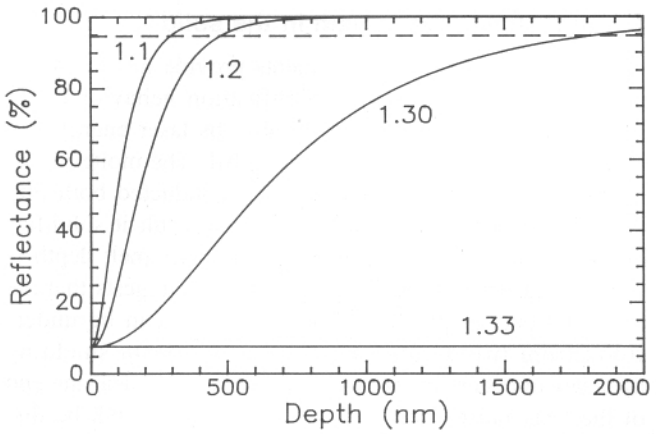

FIG. 11. Calculated reflectivity for p polarized light for an ambient/thin-film/Si system as a function of thin film thickness. Results for several refractive indices of the thin film (indicated in the figure) are compared.

can be seen, total reflection (taken as reflectivity > 95%) occurs at the water/thin film interface for a minimum film thickness depending on index: 300 nm for an index of 1.1 and 1800 nm for an index of 1.30.

b. Relation between state and optical properties for water. Using the above simulations, absolute reflectance measurements can be correlated to the effective refractive index and thickness of the simulated thin film at the interface. The relation between index and the physical state of the thin film will be discussed now. There are four different water states deviating from that at room temperature: (1) (super)heated liquid water, (2) steam, (3) high pressure water, and (4) ionized water (plasma phase). For temperatures and pressures above those at the critical point[49] (374 °C, 218 bar), (super)heated water and steam cannot be distinguished. The temperature dependence of the refractive index is weak, whereas density (pressure) fluctuations largely influence the index. In first order the index is related to the density by the theoretical Lorentz-Lorenz relation[55]:

$$(n^2 - 1)/(n^2 + 2)\rho = \text{constant}, \qquad (2)$$

where ρ is the density of the medium.

(1) The index for water at 1 bar is 1.33 at room temperature and 1.31 at 100 °C.[49] A minimum index for liquid (super)heated water occurs at the critical point and is 1.1.

(2) The index for saturated steam at 100 °C and 1 bar is 1.0. A maximum index for saturated steam is 1.1, at the critical point. For super-critical conditions, temperature and pressure determine the index, the value being larger than 1.0.

(3) The index for liquid water at room temperature is known to increase with applied pressure.[56,57] Given the pressure-density relation, the index can be calculated from formula (1). Extrapolation of data obtained from shock wave experiments[57] suggests that the index increases from 1.33 at 1 bar to 1.5 at 30 kbar.

(4) For water ionized to the plasma state the index is less than 1.33, the precise value depending on the degree of ionization.[58]

C. Transmission electron microscopy

A cross-section TEM micrograph of a sample irradiated under water is shown in Fig. 12 as a bright-field image with the corresponding diffraction pattern from the Si

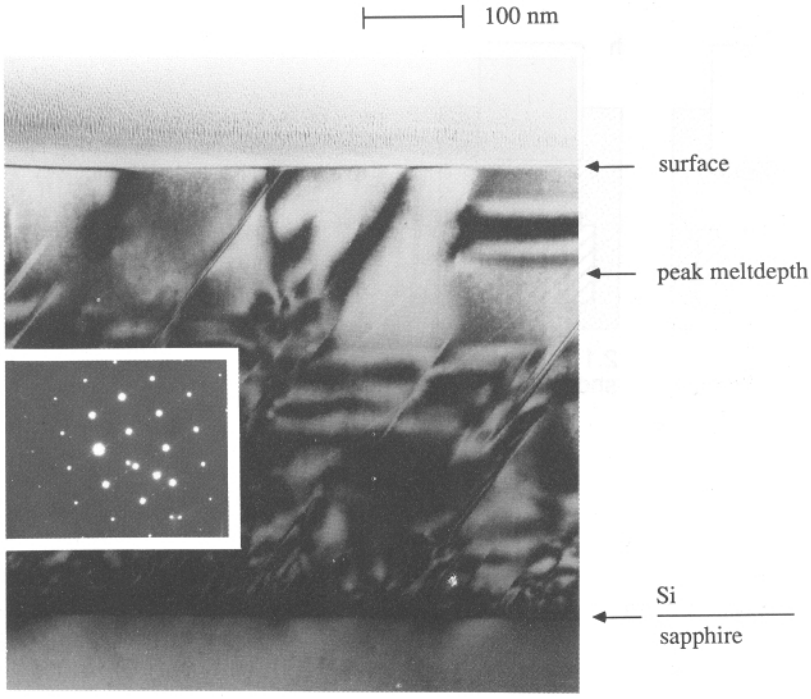

FIG. 12. Bright-field cross-sectional TEM image of an SOS sample irradiated under water. The inset shows a diffraction pattern from the Si surface region.

surface region. The large density of microtwins is normal in the highly strained silicon-on-sapphire heteroepitaxy. The maximum melt depth in this sample was determined from a transient conductance measurement to be 110 nm. From the diffraction pattern it can be concluded that the molten layer has solidified epitaxially and no surface nucleation has occurred. Within the microscope resolution of ≈40 Å, no surface oxide is observed on the sample irradiated under water. Furthermore, the Si surface appears to remain planar following solidification.

IV. DISCUSSION

Figure 13 gives a schematic overview of the sequence of phase transformations occurring in both Si and water upon irradiation. It is meant to illustrate the detailed discussion of the distinct processes in the following sections.

A. Quenching mechanism in the solid

The conductance measurements provide the following picture for the Si melt and solidification behavior under water. During irradiation, the Si absorbs laser energy and is rapidly heated and melted [Fig. 13(b)]. The molten layer is quenched as heat from the melt is conducted both into the solid Si and into the water and as a result it solidifies [Figs. 13(c) and (d)]. Under water the peak melt depth is obtained earlier in time than in air, which suggests that the absorbed energy pulse is shortened. This can be understood from two arguments. (1) A laser beam shielding mechanism occurs in the water at the interface near the end of the laser pulse. This is indeed the case, as will be discussed in the next section. (2) Heat flow from the Si to the water *during* the laser pulse reduces the amount of energy available for melting and shortens the duration of the effectively absorbed energy pulse which contributes to melt-

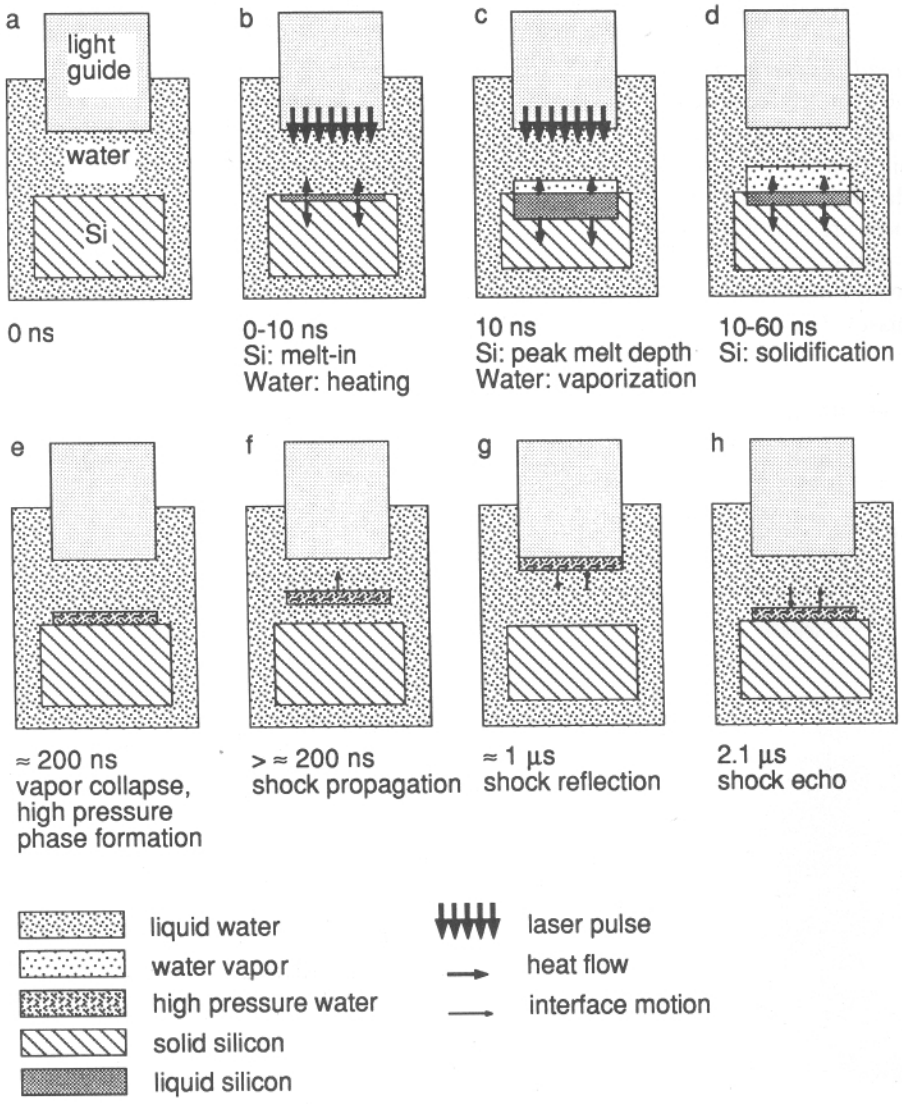

FIG. 13. Schematic of the sequence of phase transformations at the Si–H_2O interface upon pulsed laser irradiation.

ing. This is in agreement with the thermal modeling in Sec. III.A.2.a.

The effective pulse shortening results in enhancement of the quench rate due to the enhanced thermal gradient in the solid [$(\partial T/\partial z)$ term in (1)]. However, computer simulations show that a quench rate enhancement from 5.2 to 6.8 m/s for 270 nm deep melts cannot be understood from such an effect only: even a pulse shortening from 4 to 1 ns FWHM results in an enhancement of the average quench rate of only 0.7 m/s. This implies that heat flow into the water during solidification [Q term in (1)] is an additional and important term in the heat flow balance, resulting in a further enhancement of the solidification velocity.

This result has important implications for other work. Earlier, it has been shown that impurity redistribution in the Si liquid phase is reduced when the sample is irradiated under water,[59] which is now supported by the reduction in integral melt duration as is directly observed in this work. Such quenching mechanisms also clearly explain results of Ogale and co-workers[35]: using 30 ns FWHM pulses they synthesized new metastable solid solutions of the Fe–Al system as well as novel amorphous Fe–B phases by processing samples in liquid ambient. It should be noted that the absolute value of quench rate enhancement found in our present work using short laser pulses (4 ns FWHM) is relatively small. The effect might depend on laser pulse length, and the data in Ref. 59 suggest that the relative quench rate enhancement will be larger when longer pulses are used.

B. Transient phase transformation in the water

Variations in the reflectance present a real time probe of the modified properties and hence the phase changes in the water. The distinct high- and low-reflectivity regions in the reflectivity measurements will be discussed hereafter with the aid of the modeling introduced in Sec. III.B.2.

1. 0–50 ns time regime

The measured high s and p reflectivity plateaus [Fig. 5(a)] correspond to one unique region in the reflectivity simulations presented in Fig. 10. These calculations of the reflectance of the water/thin-film/Si layer structure show that both reflectivities are high if the effective index of the thin film (formed at the Si-water interface) is lower than that of water at room temperature. The data indicate that total reflection occurs at the water/thin-film interface which, according to the calculations, corresponds to a decrease in index to below 1.30. There are three possible phases which correspond to such an index: (1) (super) heated water, (2) steam, or (3) a plasma phase. Once total reflection occurs, the probe beam does not monitor the Si surface. This explains why the Si surface liquid-solid transformation is not observed. Slight nonplanarity of the reflecting interfaces and inaccuracy in the absolute reflectivity levels would explain the deviation from exactly 100%. From the timing of the leading edge of the p reflectance we see that the total reflection condition is satisfied $\approx$10 ns after the peak of the laser pulse.

The simulations of reflectivity as a function of film thickness give further insight into the nature of the phase transformations at the interface. First the possibility of (super)heated water to be formed will be discussed. A minimum index for (super)heated water is the index at the critical point, which is 1.1. From Fig. 11 it follows that for total reflection to occur at a phase with index 1.1, at least a layer thickness of 300 nm has to be formed. However, the thermal diffusion length in (heated) water after the heating time of $\approx$10 ns is in the order of only 40 nm. Although this layer will expand by thermal expansion, it is too thin to account for total reflection. Therefore, if convective motions in the liquid at the interface (which could enhance the heat coupling efficiency) are assumed not to occur, the possibility of superheated water to be the explanation of the high reflectivity plateaus can be excluded.

Steam formation is in good agreement with the observed reflectance transients. Initially, a high pressure steam phase can be formed from the thin heated water film. This steam will rapidly expand to a larger thickness, resulting in a decrease in density and thus index. The combined conditions of low index and large layer thickness can account for total reflection. During the laser pulse, formation of a transient steam phase near the Si-water interface can influence the pulsed-laser energy coupling into the sample as different conditions for reflection of the incident laser beam apply. We performed a simulation of reflectivity for the normal-incidence Nd:YAG laser beam, using the layer structure as in Fig. 9. Initially, when no steam has formed, the liquid-Si/water interface reflectivity is 66%. When a thin steam film has formed in the water at the Si surface, the total reflectivity is enhanced to at most 72%. This would imply that the fraction of the incident laser power absorbed would decrease from 34% to 28%, a decrease of 18% in power. This can result in the effective pulse shortening effect, as described in Sec. IV.A.

It should be noted that the above arguments for steam formation also hold for formation of a low-density phase above the critical temperature, which strictly may not be referred to as steam. For convenience, hereafter we shall denote this super-critical phase as steam.

Also, formation of a thin transient plasma film can account for the observed high reflectivity values. A preliminary observation by Ogale *et al.*[35] suggests that for pulsed laser irradiation of Fe under water, plasma emission from Fe or water is observed at the Fe-water interface for a time in the order of the Fe surface melt duration. Also, Ursu *et al.*[40] have found indications for plasma formation to occur at the Ti- and Zr-liquid N_2 interfaces. Although in our experiments we were not able to study possible plasma formation in detail, for completeness we will show here-

after on the basis of theoretical arguments, that indeed such transient plasma formation could occur in the water. It has been shown that highly focused (GW/cm^2) pulsed laser beams can instantly ionize water by a breakdown mechanism when the AC electric field strength is in the order of several MV/cm.[60] Multiphoton ionization, field ionization, or laser coupling to dust particles or low ionization potential impurities would initiate the process, i.e., supply sufficient free electrons. In the AC electric field these electrons can cause impact ionization followed by avalanche multiplication which would result in breakdown, i.e., transient plasma formation.[60–63] Indeed, in our experiments multi-photon ionization of water molecules could play a role at the laser peak intensity of $I = 9 \times 10^7$ W/cm^2.[64] To study the possibility of field ionization as a triggering process for breakdown, we calculate the AC electric field strength in the bulk liquid in our experiments, given by

$$E = (2 \cdot I \cdot n/\varepsilon_r \cdot c)^{1/2}, \quad (3)$$

where I is the laser intensity (9×10^7 W/cm^2), c the velocity of light, n the water refractive index (1.33), and ε_r the relative dielectric constant of water (80).[49] Using Eq. (3) we find $E = 3 \times 10^5$ V/cm, which is too low to result directly in field ionization. However, once the process is triggered such a field strength can result in impact ionization and subsequent breakdown. This will become more pronounced at or near the Si-water interface where vapor has formed with a lower dielectric constant and consequently a higher electric field strength. Steam formation would then be essential for breakdown to occur. Such effects have been found earlier by Krasucki.[65] We expect the lifetime of a laser-induced plasma phase to be in the order of the laser pulse duration due to the strong plasma cooling by the water. During the laser pulse, formation of a transient plasma phase near the Si-water interface can strongly influence the energy coupling into the sample by "plasma shielding"; i.e., as soon as it has formed the plasma reflects the laser light, which causes an effective shortening of the laser pulse. This mechanism has recently been proposed by Schoeffmann *et al.*[66] for focused irradiation in a bulk liquid.

From the above, we conclude that steam formation can explain the reflectance data in the 0–50 ns regime [Figs. 13(c) and (d)]. Formation of this phase occurs in the second half of the laser pulse and possibly initiates a short plasma phase in the water. The observation of steam or plasma phases supports the laser pulse shielding argument made in Sec. IV.A to explain the effective laser pulse shortening.

2. 200–1000 ns time-regime

Both *s* and *p* reflectivity decrease discontinuously, 200 ns after the laser pulse [Fig. 5(b)]. Apparently, suddenly the total reflection condition is then lost, indicating that the steam layer has collapsed, probably by instant condensation. Felix and Ellis[63] have earlier proposed 'vapor collapse' effects induced by laser irradiation in bulk liquids, and indeed our data give experimental evidence for such effects to occur at the solid-liquid interface. After this collapse, especially the *s* reflectivity continues to deviate substantially from the initial level before irradiation, whereas the *p* reflectance returns to the starting level. These measured reflectivity levels correspond to one unique region in the reflectivity simulations presented in Fig. 10: the effective index of the thin film (formed at the Si-water interface) must be higher than that of water at room temperature. This implies that a high-pressure phase of water has formed near the Si surface [Fig. 13(e)].

3. 1.0–5.0 μs time-regime

To study the pressure effects in more detail, microsecond timescale measurements were performed (Fig. 7). The first dip in *s* reflectivity in Fig. 7 corresponds to the dip starting at $t = 200$ ns in Fig. 5, but is less pronounced due to the fact that a lower irradiation energy density is used. The dip duration consequently is shorter: ≈800 ns. The echo effects in the pressure dip suggest that an acoustic wave is propagating through the fluid and is reflected by the lightguide end [Figs. 13(f) through (h)]. This is corroborated by the fact that the obtained apparent propagation velocity is nearly the sound velocity in (liquid) water. These observations also explain the small oscillations being superimposed on the signal in the experiments described in Fig. 5(b). There the sample-diffusor distance was only 0.6 mm and the round trip time is less than the total duration of the low reflectivity phase, resulting in superposition of acoustical reflections on the signal.

We suggest that the high pressure effects are initiated by the ultra-rapid phase transformations in the water near the Si surface. Thermal expansion, steam formation and expansion, as well as dielectric breakdown processes can result in formation of a compressive shock. Shock wave and related effects have been described in the literature for beams focused in bulk liquids[63,66–70] and at liquid gas[71] and solid-gas interfaces[72,73] (laser-ablation experiments). To our knowledge transient shock processes at the liquid-solid interface have never been studied.

The acousto-optical measurements give an indication of the absolute shock pressures in our experiments. Feiock and Goodwin[74] have performed numerical simulations of the laser-induced stresses in water and showed that shock effects in water comprise two combined pressure waves: a precursor wave due to a thermal expansion wave followed by a larger pulse with a pressure in the kbar range due to vaporization. Other authors have found substantially higher shock pressures in water, up to 200 kbar.[68] From the apparent shock propagation velocity in our experiments the shock pressure can be estimated using the equation by Walsh and Rice[57]

$$U_s - U_0 = 25306 \cdot \log(1 + U_p/5190) \quad (4)$$

and the conservation equation

$$P_1 = P_0 + \rho_0 \cdot U_s \cdot U_p \quad (5)$$

where P_1 is the pressure directly behind the leading edge of the shockfront, P_0 and ρ_0 are pressure and density ahead of the shock, U_0 is sound velocity at 1 atm and room temperature, i.e., 1483 m/s, and U_s and U_p are shock velocities and particle velocity in m/s, respectively. Using Eqs. (4) and (5) the shock velocity obtained from Fig. 8 can be converted to pressure: $P_1 = 0.4 \pm 0.3$ kbar. As the shock velocity could not be obtained accurately, the obtained pressure value has large error bars. The calculated pressure is the steady state pressure in the shock. During initiation of the shock transient higher pressures can be obtained.[69]

C. Surface structure and interface reactivity

1. Surface structure

The cross-section TEM results reveal that during solidification under water no surface nucleation has occurred in the liquid Si layer. Heat flow arguments (Sec. III.A.2.c) show that in this case the surface is undercooled 125 K with respect to the crystalline Si melting temperature. Thermodynamically, such undercooling could result in nucleation of (poly-) crystalline Si. Under the present experimental conditions of short surface melt duration apparently the kinetic conditions for nucleation are not favored. This has also been observed in experiments in air, where similar undercoolings did not result in surface nucleation for the same melt duration.[48,75]

2. Interface reactivity

The cross-section TEM results reveal that no significant oxygen incorporation has occurred in the samples which have been irradiated under water. Rutherford Backscattering Spectrometry (RBS) data for samples irradiated under water similarly have shown that indeed the integral oxygen amount in the samples was 4×10^{15} at/cm^2 for both samples irradiated in air and in water.[59] This corresponds to a few monolayers and is consequently invisible for TEM as performed here. Also, using channeling-RBS it is found that perfect epitaxy of the molten layers is obtained after solidification under water,[59] again in agreement with the present TEM results. In addition, these TEM data show that the surface morphology is not disturbed during irradiation under water.

These arguments give evidence that pulsed-laser irradiation under water induces no net chemical reactions at the Si-water interface. This observation is in contrast with many experiments for other combinations of solid substrates and liquids where a significant amount of reaction is known to occur.[30–40] Two arguments can explain the inertness of the present reaction system: (1) oxygen has a low solubility in liquid Si and (2) a native surface SiO_2 layer acts as a diffusion barrier for atomic or molecular oxygen to penetrate into the bare Si and form chemical bonds.[25,76] This oxide has a higher melting temperature than crystalline Si[$T_m(SiO_2) = 1976$ K,[49] $T_m(Si) = 1683$ K[49]] and can remain solid at laser intensities just above the Si melt threshold.[77] The validity of argument (2) could be tested by performing experiments on samples with different SiO_2 layer thicknesses. This has not yet been done.

Several interesting results have been obtained for pulsed-laser irradiation of Si in gaseous oxygen ambient at energy densities above the Si melt threshold,[23–26,76,78–80] and can be applied to our situation. In these experiments the presence of the native oxide on the substrate was of critical importance for interface reactions to occur or not. Only for extended, multiple-pulse irradiation (integral irradiation time in the order of minutes) oxygen diffusion through a surface oxide becomes significant. In contrast, on samples where the native oxide was etched off prior to irradiation a surface layer can be oxidized in oxygen ambient with one laser pulse.[25] Liu *et al.*[26] and Berti *et al.*[23,78] have reported that large amounts of oxygen from the gas phase can be incorporated in Si covered by an oxide only when the irradiation energy density is well above the Si melt threshold. Under these conditions the native oxide is evaporated during irradiation.[23,78] After significant evaporation (hence at temperatures far above the melting point) an interface reaction between Si and oxygen can start whereupon transport to deeper regions takes place by convective motions. The driving force for these motions would be surface-tension gradients induced by evaporation of the oxide. In our present experiments such convective motions have not occurred as appears from the observed microstructure; these would have resulted in large surface roughness after solidification. This implies that the oxide is not evaporated in our experiments. This can be understood from the arguments that (1) evaporation conditions for a surface oxide in contact with a liquid medium are different, (2) the energy density used is relatively low, and (3) the water layer has a cooling effect at the interface which reduces the evaporation rate.

Several experiments have been performed in which laser irradiation at the solid-gas, solid-liquid, or solid-solid interface was performed for dopant incorporation. Reactive gaseous and liquid environments studied until now are hydride, chloride, or organic compounds containing the dopant species.[27–29,32,81–88] In these experiments generally decomposition of gas molecules by pyrolysis or photolysis is suggested for reactive dopant atoms to be formed. Then diffusion limited transport accounts for the observed deep penetration into the molten solid, which upon solidification is followed by substitutional incorporation of the dopants. Also, thin mono-atomic solid films of P, B, Al, Sb, Ga, Bi, and In deposited or absorbed on Si substrates have

been irradiated.[89–94] Here also it has been shown that atoms from the deposited mono-atomic solid film diffuse into a shallow molten surface region of the Si substrate. It is interesting to compare the general observation in these doping experiments to those presently observed for the Si-water system. Although in many of the above-mentioned solid-gas, solid-liquid, and solid-solid experiments the Si surface native oxide was etched off prior to the experiments, in several other experiments this was not the case. Still, a significant interface reaction occurred for these cases. Apparently for these types of reactions the native SiO_2 layer is not crucial for a reaction to occur or not, in contrast to the effect observed for irradiation under water. We suggest that this can be understood from the difference in reactivity of the heated gas, liquid, or solid media near the Si surface. Reactive environments can enhance dissolution of the surface oxide whereupon a reaction at the bare liquid Si surface can take place.

V. CONCLUSIONS

In conclusion, we have been able to unravel the transient processes in both media at the Si–H_2O interface upon nanosecond pulsed laser irradiation. During irradiation the Si absorbs laser energy and is rapidly heated and melted. Heat from the melt is transported to the water. Optical measurements suggest that this results in formation of a steam or a low-density super-critical phase at the interface. The typical formation time is 10 ns. During formation this phase rapidly expands, whereupon it suddenly collapses after 200 ns. A more detailed investigation, e.g., using different wavelengths or a different probe laser geometry, is required to characterize the nature of this phase in more detail. Rapid phase transformations in the water initiate a high pressure shock wave in the water. The steady state shock pressure is 0.4 ± 0.3 kbar.

Transient phase transformations which influence the energy coupling into the sample, as well as heat flow into the water during the laser pulse, result in an effective laser pulse shortening. This is directly observed from the Si melt-in behavior. Pulse shortening as well as heat flow into the water during solidification result in an enhancement of the solidification velocity by up to 30% for deep melts. All these observations are corroborated by standard heat flow estimates. These quench rate enhancement effects, which have been suggested by several workers, are now for the first time directly observed.

After irradiation the Si-water interface has remained planar. No surface nucleation has occurred during solidification and no significant chemical reactions have occurred at the interface. The Si surface native oxide could play a crucial role in the kinetics of the interface reactions: it is suggested that, for the irradiation intensity studied, no evaporation of the oxide occurs and it therefore acts as a reaction barrier.

The presently observed fundamental phenomena give insight into the mechanisms behind various results on laser-induced synthesis at solid-liquid interfaces reported recently in the literature. It is now for the first time directly observed that in such reactions high temperature vapor phases of the liquid may be responsible for the reaction with the solid and that pressure-induced effects can play a role.

ACKNOWLEDGMENTS

Scott Stiffler (Cornell University) is acknowledged for performing TEM analysis. The Dutch contribution to this work is part of the research program of the Stichting voor Fundamenteel Onderzoek der Materie (FOM, Foundation for the Fundamental Research on Matter) and was made possible by financial support from the Stichting voor Technische Wetenschappen (STW, Foundation for the Advancement of Technical Sciences) and the Nederlandse Organisatie voor Wetenschappelijk Onderzoek (NWO, Netherlands Organization for the Advancement of Research). Work at Cornell was supported by the National Science Foundation through the Materials Science Center. Samples were fabricated at the National Nanofabrication Facility at Cornell (NSF).

REFERENCES

[1] *Laser Annealing of Semiconductors*, edited by J. M. Poate and J. W. Mayer (Academic, New York, 1982).
[2] D. H. Lowndes, S. J. Pennycook, G. E. Jellison, Jr., S. P. Withrow, and D. N. Mashburn, J. Mater. Res. **2**, 648 (1987).
[3] R. F. Wood and G. A. Geist, Phys. Rev. B **34**, 2606 (1986).
[4] M. O. Thompson and P. S. Peercy, in *Beam-Solid Interactions and Phase Transformations*, edited by H. Kurz, G. L. Olson, and J. M. Poate (MRS Symp. Proc., MRS, Pittsburgh, PA, 1986), p. 99.
[5] M. O. Thompson and P. S. Peercy, in *Beam-Solid Interactions and Transient Processes*, edited by M. O. Thompson, S. T. Picraux, and J. S. Williams (MRS Symp. Proc., MRS, Pittsburgh, PA, 1987), Vol. 74, p. 15.
[6] M. J. Aziz, J. Y. Tsao, M. O. Thompson, P. S. Peercy, and C. W. White, Phys. Rev. Lett. **56**, 2489 (1986).
[7] M. J. Aziz and C. W. White, Phys. Rev. Lett. **57**, 2675 (1986).
[8] S. U. Campisano, D. C. Jacobson, J. M. Poate, A. G. Cullis, and N. G. Chew, Appl. Phys. Lett. **46**, 846 (1985).
[9] P. S. Peercy, M. O. Thompson, and J. Y. Tsao, Appl. Phys. Lett. **47**, 244 (1985).
[10] P. S. Peercy, M. O. Thompson, J. Y. Tsao, and J. M. Poate, see Ref. 4, p. 125.
[11] J. J. P. Bruines, R. P. M. van Hal, H. M. J. Boots, W. Sinke, and F. W. Saris, Appl. Phys. Lett. **48**, 1252 (1986).
[12] J. J. P. Bruines, R. P. M. van Hal, H. M. J. Boots, A. Polman, and F. W. Saris, Appl. Phys. Lett. **49**, 1160 (1986).
[13] D. H. Lowndes, G. E. Jellison, Jr., S. J. Pennycook, S. P. Withrow, and D. N. Mashburn, Appl. Phys. Lett. **48**, 1389 (1986).
[14] W. Sinke and F. W. Saris, Phys. Rev. Lett. **53**, 2121 (1984).
[15] J. Narayan and C. W. White, Appl. Phys. Lett. **44**, 35 (1984).
[16] P. M. Richards, Phys. Rev. B **38**, 2727 (1988).
[17] J. Y. Tsao, M. J. Aziz, M. O. Thompson, and P. S. Peercy, Phys. Rev. Lett. **56**, 2712 (1986).

[18]J. Y. Tsao and P. S. Peercy, Phys. Rev. Lett. **58**, 2782 (1987).
[19]G. E. Jellison, Jr., D. H. Lowndes, D. N. Mashburn, and R. F. Wood, Phys. Rev. B **34**, 2407 (1986).
[20]S. R. Stiffler and M. O. Thompson, Phys. Rev. Lett. **60**, 2519 (1988).
[21]R. F. Wood and G. E. Giles, Phys. Rev. B **23**, 2923 (1981).
[22]R. F. Wood and G. E. Giles, Phys. Rev. Lett. **57**, 873 (1986).
[23]M. Berti, L. F. Doná dalle Rose, A. V. Drigo, C. Cohen, J. Siejka, G. G. Bentini, and E. Jannitti, Phys. Rev. B **34**, 2346 (1986).
[24]C. Cohen, J. Siejka, M. Berti, A. V. Drigo, G. G. Bentini, D. Pribat, and E. Jannitti, J. Appl. Phys. **55**, 4081 (1984).
[25]K. Hoh, H. Koyama, K. Uda, and Y. Miura, Jpn. J. Appl. Phys. **19**, 375 (1980).
[26]Y. S. Liu, S. W. Chiang, and F. Bacon, Appl. Phys. Lett. **38**, 1005 (1981).
[27]G. B. Turner, D. Tarrant, G. Pollock, R. Pressley, and R. Press, Appl. Phys. Lett. **39**, 967 (1981).
[28]G. G. Bentini, M. Biaconi, L. Correra, R. Nipoti, C. Summonte, C. Cohen, and J. Siejka, in *Photon, Beam and Plasma Enhanced Processing*, edited by A. Golanski, V. T. Nguyen, and E. F. Krimmel (E-MRS Symp. Proc. XV), (Les Editions de Physique, Les Ulis, France, 1987), p. 273.
[29]T. F. Deutsch, J. C. C. Fan, G. W. Turner, R. L. Chapman, D. J. Ehrlich, and R. M. Osgood, Jr., Appl. Phys. Lett. **38**, 144 (1981).
[30]K. Nakamura, M. Hikita, H. Asano, and A. Terada, Jpn. J. Appl. Phys. **21**, 672 (1982).
[31]S. B. Ogale, A. Polman, F. O. P. Quentin, S. Roorda, and F. W. Saris, Appl. Phys. Lett. **50**, 138 (1987).
[32]R. Stuck, E. Fogarassy, J. C. Muller, M. Hodeau, A. Wattiaux, and P. Siffert, Appl. Phys. Lett. **38**, 715 (1981).
[33]S. Roorda, A. Polman, S. B. Ogale, and F. W. Saris, in *Photon, Beam and Plasma Stimulated Chemical Processes at Surfaces*, edited by V. M. Donnelly, I. P. Herman, and M. Hirose (MRS Symp. Proc., MRS, Pittsburgh, PA, 1987), Vol. 75, p. 297.
[34] P. P. Patil, D. M. Phase, S. A. Kulkarni, S. V. Ghaisas, S. K. Kulkarni, S. M. Kanetkar, S. B. Ogale, and V. G. Bhide, Phys. Rev. Lett. **58**, 238 (1987).
[35]S. B. Ogale, P. P. Patil, D. M. Phase, Y. V. Bhandarkar, S. K. Kulkarni, S. Kulkarni, S. V. Ghaisas, S. M. Kanetkar, V. G. Bhide, and S. Guha, Phys. Rev. B **36**, 8237 (1987).
[36]S. V. Ghaisas, A. P. Malshe, P. P. Patil, S. M. Kanetkar, S. B. Ogale, and V. G. Bhide, J. Appl. Phys. **62**, 2799 (1987).
[37]S. B. Ogale, P. P. Patil, S. Roorda, and F. W. Saris, Appl. Phys. Lett. **50**, 1802 (1987).
[38]S-W. Chan, D. Dijkkamp, X. D. Wu, T. Venkatesan, and C. C. Chang, see Ref. 33, p. 287.
[39]D. Dijkkamp, X. D. Wu, S-W. Chan, and T. Venkatesan, see Ref. 33, p. 303.
[40]I. Ursu, I. N. Mihailescu, L. Nanu, L. C. Nistor, M. Popescu, V. S. Teodorescu, A. M. Prokhorov, V. I. Konov, S. A. Uglov, and V. G. Ralchenko, J. Phys. D: Appl. Phys. **19**, 1183 (1986).
[41]A. Polman, W. Sinke, F. W. Saris, M. J. Uttormark, and M. O. Thompson, Appl. Phys. Lett. **52**, 535 (1988).
[42]P. L. Liu, R. Yen, N. Bloembergen, and R. T. Hodgson, Appl. Phys. Lett. **34**, 864 (1979).
[43]S. U. Campisano, D. C. Jacobson, J. M. Poate, A. G. Cullis, and N. G. Chew, Appl. Phys. Lett. **45**, 1216 (1984).
[44]G. J. Galvin, M. O. Thompson, J. W. Mayer, P. S. Peercy, R. B. Hammond, and N. Paulter, Phys. Rev. B **27**, 1079 (1983).
[45]*Liquid Semiconductors*, edited by V. M. Glazov, S. N. Chizhevskaya, and N. N. Glagoleva (Plenum, New York, 1969).
[46]A. G. Cullis, H. C. Webber, and P. Bailey, J. Phys. E: Sci. Instrum. **12**, 688 (1979).
[47]D. H. Auston, C. M. Surko, T. N. C. Venkatesan, R. E. Slusher, and J. A. Golovochenko, Appl. Phys. Lett. **33**, 437 (1978).
[48]M. O. Thompson, "Liquid-Solid Interface Dynamics During Pulsed Laser Melting of Silicon-On-Sapphire," Ph.D. Thesis (Cornell University, Ithaca, NY, 1984).
[49]*CRC Handbook of Chemistry and Physics* (Chemical Rubber Company, Boca Raton, FL, 1981).
[50]M. O. Thompson, P. H. Bucksbaum, and J. Bokor, in *Energy-Beam Solid Interactions and Transient Thermal Processing*, edited by D. K. Biegelsen, G. A. Rozgonyi, and C. V. Shank (MRS Symp. Proc., MRS, Pittsburgh, PA, 1985), Vol. 35, p. 181.
[51]J. Y. Tsao, M. J. Aziz, P. S. Peercy, and M. O. Thompson, in *Fundamentals of Beam-Solid Interactions and Transient Thermal Processing*, edited by M. J. Aziz, L. E. Rehn, and B. Stritzker (MRS Symp. Proc., MRS, Pittsburgh, PA, 1988), Vol. 100, p. 519.
[52]J. Y. Tsao, M. J. Aziz, M. O. Thompson, and P. S. Peercy, Phys. Rev. Lett. **56**, 2712 (1986).
[53]R. M. A. Azzam and N. M. Bashara, *Ellipsometry and Polarized Light* (North-Holland, Amsterdam, 1987).
[54]R. F. Wood, C. W. White, and R. T. Young, in *Semiconductors and Semimetals*, Vol. 23, *Pulsed Laser Processing of Semiconductors* (Academic, New York, 1984).
[55]M. Born and E. Wolf, *Principles of Optics* (Pergamon, New York, 1968).
[56]Landolt-Börnstein, *Eigenschaften der Materie in ihren Aggregatzuständen, 8. Teil* (Springer, Berlin, 1962).
[57]J. M. Walsh and M. H. Rice, J. Chem. Phys. **26**, 815 (1957).
[58]P. C. Clemmov and J. P. Dougherly, *Electrodynamics of Particles and Plasmas* (Addison-Wesley, Reading, MA, 1969).
[59]A. Polman, S. Roorda, S. B. Ogale, and F. W. Saris, see Ref. 5, p. 129.
[60]S. R. J. Brueck and H. Kildal, J. Appl. Phys. **52**, 1004 (1981).
[61]G. A. Hill, D. J. James, and S. A. Ramsden, J. Phys. D: Appl. Phys. **5**, 155 (1972).
[62]N. Bloembergen, IEEE J. Quantum Electron. **QE-10**, 375 (1974).
[63]M. P. Felix and A. T. Ellis, Appl. Phys. Lett. **19**, 484 (1971).
[64]V. S. Letokhov, *Laser Photoionization Spectroscopy* (Academic, Orlando, 1987).
[65]Z. Krasucki, Proc. R. Soc. London. Ser. A **294**, 393 (1966).
[66]H. Schoeffmann, H. Schmidt-Kloiber, and E. Reichel, J. Appl. Phys. **63**, 46 (1988).
[67]D. C. Emmony, M. Siegrist, and F. K. Kneubühl, Appl. Phys. Lett. **29**, 547 (1976).
[68]C. E. Bell and J. A. Landt, Appl. Phys. Lett. **10**, 46 (1967).
[69]C. E. Bell and B. S. Maccabee, Appl. Opt. **13**, 605 (1974).
[70]D. Salzmann, I. Gilath, and B. Arad, Appl. Phys. Lett. **52**, 1128 (1988).
[71]A. N. Pirri, R. G. Root, and P. K. S. Wu, AIAA J. **16**, 1296 (1978).
[72]G. Koren, Appl. Phys. Lett. **51**, 569 (1987).
[73]R. E. Walkup, J. N. Jasinski, and R. W. Dreyfus, Appl. Phys. Lett. **48**, 1690 (1986).
[74]F. D. Feiock and L. K. Goodwin, J. Appl. Phys. **43**, 5061 (1972).
[75]S. R. Stiffler, M. O. Thompson, and P. S. Peercy, Phys. Rev. Lett. **60**, 2519 (1988).
[76]A. Cros, F. Salvan, and J. Derrien, Appl. Phys. A **28**, 241 (1982).
[77]Z. L. Wang, J. F. M. Westendorp, and F. W. Saris, Nucl. Instrum. Methods **211**, 193 (1983).
[78]M. Berti, A. V. Drigo, G. G. Bentini, C. Cohen, J. Siejka, and E. Jannitti, in *Energy Beam–Solid Interactions and Transient Thermal Processing*, edited by V. T. Nguyen and A. G. Cullis (Les Editions de Physique, Les Ulis Cedex, 1985), p. 131.
[79]H. Richter, T. E. Orlowski, M. Kelly, and G. Margaritondo, J. Appl. Phys. **56**, 2351 (1984).
[80]Y. S. Liu, S-W. Chiang, and W. Katz, in *Laser and Electron-Beam Interactions with Solids*, edited by B. R. Appleton and G. K. Keller (Elsevier, Amsterdam, 1982).
[81]J. C. C. Fan, T. F. Deutsch, G. W. Turner, D. J. Ehrlich, R. L. Chapman, and R. M. Osgood, in *Proc. 15th IEEE Photovoltaic Specialists Conference* (IEEE, New York, 1981), p. 432.
[82]T. F. Deutsch, D. J. Ehrlich, D. D. Rathman, D. J. Silversmith, and

R. M. Osgood, Jr., Appl. Phys. Lett. **39**, 825 (1981).
[83]G. B. Turner, D. Tarrant, D. Aldrich, R. Pressley, and R. Press, in *Proc. 4th E. C. Photovoltaic Specialists Conference* (Reidel, Dordrecht, 1982), p. 427.
[84]G. B. Turner, D. Tarrant, D. Aldrich, R. Pressley, and R. Press, in *Proc. 16th IEEE Photovoltaic Specialists Conference* (IEEE, New York, 1982), p. 775.
[85]P. G. Carey, J. E. Turner, K. Nauka, G. A. Reid, and T. W. Sigmon, in *Rapid Thermal Processing of Electronic Materials*, edited by S. R. Wilson, R. Powell, and D. E. Davies (MRS Symp. Proc., MRS, Pittsburgh, PA, 1987), Vol. 92, p. 65.
[86]G. G. Bentini, M. Bianconi, L. Correra, R. Lotti, and C. Summonte, in *Proc. 7th E. C. Photovoltaic Solar Energy Conference*, edited by A. Goetzberger, W. Palz, and G. Wileke (Reidel, Dordrecht, 1987), p. 1044.
[87]T. W. Sigmon, P. G. Carey, R. L. Press, T. S. Fahler, and R. J. Pressley, in *Energy Beam–Solid Interactions and Transient Thermal Processing*, edited by J. C. C. Fan and N. M. Johnson (MRS Symp. Proc., MRS, Pittsburgh, PA, 1984), Vol. 23, p. 247.
[88]P. G. Carey, T. W. Sigmon, R. L. Press, and T. S. Fahlen, IEEE Electron. Dev. Lett. **EDL-6**, 291 (1985).
[89]E. Fogarassy, R. Stuck, J. J. Grob, and P. Siffert, J. Appl. Phys. **52**, 1076 (1981).
[90]E. Fogarassy, R. Stuck, J. C. Muller, M. Hodeau, A. Wattiaux, M. Toulemonde, and P. Siffert, in *Proc. 3rd E. C. Photovoltaic Solar Energy Conference*, edited by W. Palz (Reidel, Dordrecht, 1981), p. 639.
[91]E. P. Fogarassy, D. H. Lowndes, J. Narayan, and C. W. White, J. Appl. Phys. **58**, 2167 (1985).
[92]K. Affolter, W. Lüthy, and M. von Allmen, Appl. Phys. Lett. **33**, 185 (1978).
[93]J. Narayan, R. T. Young, R. F. Wood, and W. H. Christie, Appl. Phys. Lett. **33**, 338 (1978).
[94]T. Sameshima, S. Usui, and M. Sekiya, J. Appl. Phys. **62**, 711 (1987).